

# A Review of Numerical Models for Predicting the Energy Deposition and Resultant Thermal Response of Humans Exposed to Electromagnetic Fields

RONALD J. SPIEGEL, MEMBER IEEE

(*Invited Paper*)

**Abstract**—For humans exposed to electromagnetic (EM) radiation, the resulting thermophysiological response is not well understood. Because it is unlikely that this information will be determined from quantitative experimentation, it is necessary to develop theoretical models which predict the resultant thermal response after exposure to EM fields. These calculations are difficult and involved because the human thermoregulatory system is very complex. In this paper, the important numerical models are reviewed and possibilities for future development are discussed.

## I. INTRODUCTION

**B**ECAUSE OF SOCIETY'S increased usage of electromagnetic (EM) radiation for a variety of purposes, it is imperative to be able to quantify both the absorption of EM energy in the human body and the resulting thermal response. Such knowledge is indispensable if one is to either selectively apply EM fields for therapeutic purposes or determine if the EM fields emitted by a radiating device are harmful. Because ethical considerations make EM exposure of humans for experimental purposes difficult, it is convenient to develop realistic models through computer simulation.

Thermally harmful effects can occur if the total EM energy absorbed by the object is large enough to cause the body's temperature control system to fail, resulting in an unregulated rise in the deep body or "core" temperature (hyperthermia). It is interesting to note that core temperature generally implies rectal temperature (also called colonic temperature in laboratory animals); however, no single internal temperature can be taken to be representative of the entire core. For humans, the oesophageal temperature probably is more indicative of a single core temperature,

since it provides a more accurate indicator of the arterial blood temperature. As a consequence of the nonuniform energy deposition produced by EM fields, it is also possible that localized temperature increases, so-called "hot-spots", can arise without any significant increase in any single measure of the core temperature. Thus, if the rectal temperature is monitored, as is usually the case in laboratory experiments involving animals, it is possible that no discernable temperature rise would be measured. However, localized temperatures above 41.6 °C can cause protein denaturation, increased permeability of cell membranes, or the liberation of toxins in the location where the hot-spot exists. The severity of the resultant physiologic effect produced by localized temperature increases can be expected to be worsened in critical organs, such as the brain.

Conversely, the heating of tissue by EM radiation has some potentially beneficial properties. For example, in recent years, a therapeutic modality in cancer treatment has involved the heating of tumor tissue. The treatment involves heating cancer cells to at least 42 °C with EM fields alone or in conjunction with x-ray radiation or chemotherapy. Many devices have been developed for producing hyperthermia; however, they can generally be grouped into two categories: regional or local. The regional devices produce EM absorption over an appreciable portion of the body where the cancerous tissue is located, and it is hoped that the temperature of the tumor is elevated to significantly higher values than the surrounding tissue. The success of this type of treatment is based on the premise that blood flow is substantially less in tumors than normal tissue or that the electric permittivity of cancerous cells is different from normal cells, resulting in enhanced EM absorption in the tumor. Localized hyperthermic strategies usually involve small EM antennas or arrays of antennas which are embedded into or around the tumors through catheters or hypodermic needles. The radiation pattern of the antennas is chosen to maximally irradiate the tumor while minimizing the exposure to the surrounding tissue.

Manuscript received October 12, 1983; revised March 5, 1984.

This paper has been reviewed by the Health Effects Research Laboratory, U.S. Environmental Protection Agency (EPA), and approved for publication. Mention of trade names or commercial products does not constitute endorsement or recommendation for use. The opinions expressed in this paper are those of the author and do not necessarily reflect official EPA opinion.

The author is with the Experimental Biology Division, Health Effects Research Laboratory, U.S. Environmental Protection Agency, Research Triangle Park, NC 27711.

The development of models to predict the absorption of EM energy and the physiologic thermoregulatory response for the human body have proceeded along different paths for several years, primarily because of little or no interaction between the involved disciplines. In general, the specialized engineering community (primarily electrical engineers) working in the EM biodosimetry area produced the necessary techniques to predict the absorption of EM energy in biological systems. Concurrently, but separately, physiologists (primarily thermal) promulgated thermoregulatory models to predict man's thermal properties under normal thermal loads consisting of different levels of exercise and environmental conditions. As might be expected, both groups advanced from relatively simple models to sophisticated ones with greater predictive capacity.

With the recent emergence of bioelectromagnetics as a distinct discipline, there has been a merging of the two areas. Each discipline is now more cognizant of the other, with the result that several rudimentary models are now described in the literature which predict the resultant thermoregulatory effect when the human body is exposed to EM radiation. This paper will discuss the state-of-the-art of the models, some unresolved problems relative to the models, and possible future development.

## II. EM DOSIMETRIC MODELS

Recent reviews [1]–[4] have summarized both experimental methodologies as well as computational models based on either analytical or numerical procedures. Consequently, the following material will not duplicate the information in these articles. Emphasis will be focused on the latest and most sophisticated numerical models. Experimental methodologies based, for example, on advanced phantom models of man or animals [5], [6] will not be covered either, because interfacing EM models and heat transfer models with a high degree of spatial resolution requires a tremendous number of data points. The practicality of experimentally acquiring this huge data base is, at present, questionable.

The central issue concerning the dosimetric assessment of the absorption of EM energy by biological subjects is: how much is absorbed and where is it deposited. This is usually quantified by the specific absorption rate (SAR), which is the mass-normalized rate of energy absorbed by the object, and is defined at a specific location by the expression

$$\text{SAR} = \frac{\sigma}{\rho} |E|^2 \quad (1)$$

where  $E$  is the RMS value of the internal field strength,  $\sigma$  is the tissue conductivity, and  $\rho$  is the tissue mass density. Thus, the localized SAR is directly related to the internal electric field and the numerical procedures all involve the determination of the electric-field distribution within the biological body.

Calculation of the internal fields is, however, difficult to achieve because they are strongly dependent on a number

of factors. For example, the nature (near- or far-zone) and frequency of the incident fields, the dimension and shape of the body, the dielectric properties of the body, and whether or not the body is well insulated from earth or grounded all play important roles in the distribution of internal fields. The mathematical techniques consist of numerically solving Maxwell's equations for reasonably accurate representations of the actual objects. Generally, two numerical methods are employed: the method of moments and finite-element or difference approaches. Large main-frame computers are usually required to solve the resulting approximations to Maxwell's equations. Inherent in each method are advantages and disadvantages, and these will be elaborated upon in the following discussion.

### A. Moment Method Models

The method of moments has been extensively utilized to calculate localized SAR's in block model representations of humans and animals [7]–[10]. For example, Fig. 1 contains a 180-cubical block model of man used by Hagmann *et al.* [9]. The blocks or cells were chosen to best fit the contour and volume of a 70-kg human within the limitations of 180 blocks. Anatomical cross-sectional data were used to portion the various kinds of tissue (bone, muscle, fat, etc.) throughout the block model.

This technique proceeds as follows. First, an integral equation for the electric field induced within the irradiated object under the influence of an incident field is derived from consideration of Maxwell's equations and the application of the appropriate boundary conditions. The internal field vector is expanded in terms of subsectional basis functions [11] and substituted into the integral equation. Next, a set of testing functions is formed, and the inner product of the new integral equation with each testing function is taken. This procedure results in an approximation of the original integral equation by a linear system of equations.

Usually, pulse expansion and delta testing functions are employed in this procedure, due to the simplicity of the resulting expressions. With pulse basis functions, it is tacitly assumed that the electric field is constant over each block. Utilizing delta testing functions implies that the electric field is calculated at the center of each block, and allows the integral equation to be expressed in matrix form as

$$[G_{mn}][E_m] = -[E_m^i] \quad (2)$$

where  $[G_{mn}]$  is the EM coupling between cells,  $[E_m]$  is the electric field induced within the object, and  $[E_m^i]$  is the incident field. For an object divided into  $N$  blocks,  $m$  and  $n$  would range from 1 to  $N$ , but  $[G_{mn}]$  is a  $3N \times 3N$  matrix because of the vector nature of the electric field. The unknown electric field at the center of each cell is obtained from (2) by employing a Gauss-Jordan elimination method. The localized SAR's for each block can then be calculated from (1).

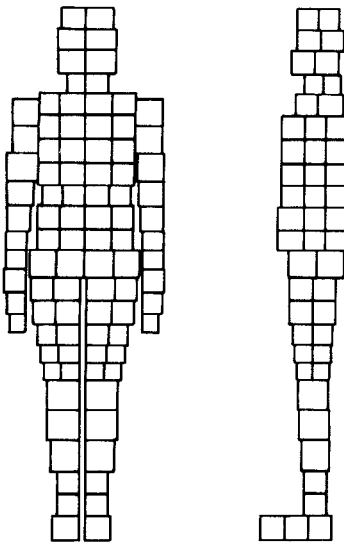


Fig. 1. A realistic block model of man [9].

The  $[G]$  matrix of (2) can be expressed in the form

$$[G_{mn}] = \begin{bmatrix} [G_{mn}^{xx}] & [G_{mn}^{xy}] & [G_{mn}^{xz}] \\ [G_{mn}^{yx}] & [G_{mn}^{yy}] & [G_{mn}^{yz}] \\ [G_{mn}^{zx}] & [G_{mn}^{zy}] & [G_{mn}^{zz}] \end{bmatrix} \quad (3)$$

where the elements of each submatrix are described elsewhere [7]. For the off-diagonal elements associated with the submatrices of (3), a Gaussian quadrature numerical integration technique can be utilized to evaluate them. When  $m = n$ , the diagonal elements of the diagonal submatrices can be evaluated by approximating the volume of each small cubical block by a small sphere of equal volume.

Although, in principle, a complete solution has been specified for virtually any type of biological body and external electric field, it may be difficult to use this method because of the large order of the  $[G]$  matrix. For example, if the object is divided into 1000 blocks, then the interaction matrix would be of order 3000 by 3000, due to the vector nature of the induced internal electric field. Thus, 9 million storage locations would be required, and a solution would be impossible even on the largest computers. It is imperative, therefore, to use ingenuity in formulating the problem so all possible storage reductions are utilized.

Fortunately, some simplifications are provided by the shape of most biological objects, i.e., the left half is a mirror image of the right half. This means that, for incident fields which are equal over each half of the object, only half the object needs to be modeled, thereby increasing the total number of cells into which the body can be partitioned. Consequently, for an object containing  $N$  cells, only a matrix of order  $3N/2$  is required to solve the problem. A significant savings of computer core is realized because  $9N^2/4$  storage locations are needed, as compared with  $9N^2$  when symmetry conditions are not included in the analysis.

Another important symmetry condition exists when the object is located over a ground plane, as illustrated by Fig. 2. The normal approach to solving this type of problem is

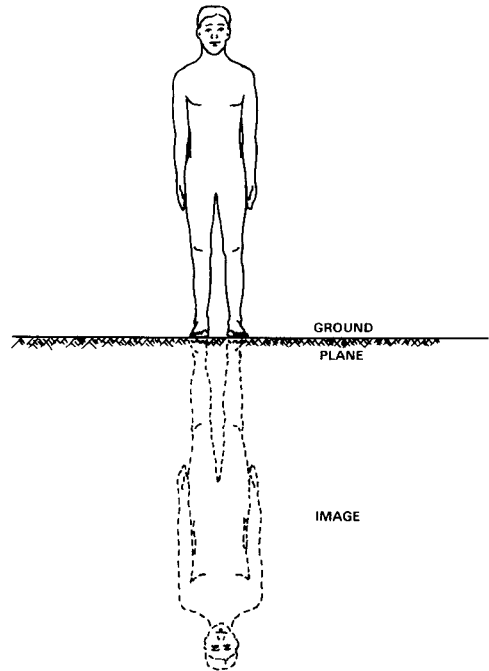


Fig. 2. Object over a ground plane.

to include the image of the object in the analysis. Clearly, if the pertinent symmetry conditions are not invoked, then twice as many cells are required as when the object is located in free-space. The necessary symmetry conditions can be determined by the application of well-known relationships for the electric field after the image plane is removed. When these symmetry conditions are utilized, storage requirements are exactly the same as in the free-space situation.

Also, it may be possible to reduce storage requirements by putting restraints on the induced electric-field components. For example, if the object is thin in any direction, then the induced component of the electric field in that direction may be smaller than the other components and, therefore, may be neglected. It goes without saying that one must be very judicious about what field components are neglected because, in general, all three components exist inside biological objects exposed to EM fields.

Fig. 3 shows some localized SAR data, as well as whole-body SAR information, as a function of frequency when the human block model is situated on a ground plane and irradiated by an EM plane-wave with its electric-field vector parallel to the long axis of the body ( $E$ -polarization). Perhaps the most important conclusion which may be drawn from these curves is that the localized SAR in the legs is approximately five times larger than the whole-body average. As will be illustrated later with the thermal model, this localized SAR will produce elevated temperatures in the legs. Note also that these results tend to imply that part-body resonances exist. For example, it is seen that resonant frequencies for the arms and head are approximately 150 and 375 MHz, respectively. Hagmann *et al.* [12] further investigated the head-resonance effect by modeling the head and neck with greater resolution by increasing the

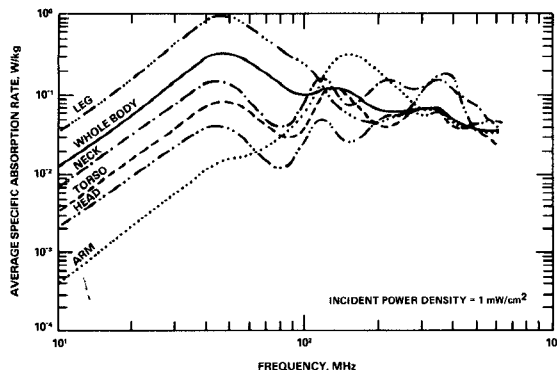


Fig. 3. Absorption for a man block model standing on a ground plane [10].

number of blocks in the head and neck region. Finally, it is worth noting that the upper bound for the block dimensions of the model is restricted by the frequency of the incident field: the higher the frequency, the smaller the block size requirement. Consequently, computer storage limitations restrict SAR calculations to an upper frequency limit of around 600 MHz.

EM absorption in block models irradiated by near-field conditions has also been investigated. Near-field exposure is probably a more realistic situation than the plane-wave case when considering the complex fields encountered in the environment. However, calculations are generally more difficult because the near-field interaction with biological objects can be extremely complicated. Thus, it is essentially impossible to draw far-reaching conclusions in regard to extrapolating results for one case to another; therefore, each situation has to be investigated separately. A study [13] involving the interaction of the human block model with a simulated leakage-field distribution for an industrial RF heat sealer has been reported. It showed that the localized SAR values are lower than for plane-wave exposure at equivalent power density levels. Others [14] have studied the localized SAR distributions when antennas (monopoles and dipoles) are placed very close to the body. As might be expected, localized SAR distributions produced by the antennas are much different than those generated by plane-wave fields.

The accuracy of these moment method solutions is very difficult to establish. Phantom experimental measurements have shown that computed whole-body or average SAR's are reasonably accurate, but localized SAR's can yield unreliable results [15]. In general, increasing the number of blocks does not always improve convergence and, consequently, the accuracy of the solution. Detailed reasons for this can be found in the mathematics associated with the method [11]. Basically, pulse functions are not well-behaved basis functions, and this leads to numerical instabilities. Physically, this amounts to EM boundary conditions not being satisfied at the interfaces between different dielectric media.

To improve the accuracy of the moment method solutions, better behaved basis functions are being utilized. New models [16], [17] which use linear basis functions and

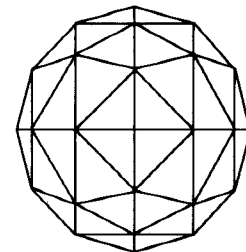


Fig. 4. Tetrahedral model of a sphere [17].

tetrahedral elements as the basic building blocks have been described. In addition to improving the convergence of the solution, the tetrahedral elements allow curved surfaces to be approximated much more accurately than is possible with cubical blocks. One apparent disadvantage of the tetrahedral approach is that the computer time required to calculate values for all the elements associated with the interaction matrix is much longer than for cubical block models, due to the fact that more numerical integrations have to be performed. To date, the tetrahedral method has been tested for accuracy by modeling elementary shapes such as spheres [17]. A tetrahedral approximation to a sphere is shown in Fig. 4. While the calculated internal field distributions for these shapes are in close agreement with other accepted calculations, the accuracy of the method is not presently known for simulations of complex, biological bodies.

### *B. Finite-Difference Models*

The finite-difference method is finding increased usage for calculating the interaction of EM fields with complex, lossy dielectric bodies. This method's funding genesis and development has occurred primarily under the auspices of the U.S. Department of Defense in order to determine how a nuclear EM pulse (EMP) interacts with and penetrates into various military equipment, such as missiles and aircraft. The finite-difference method possesses inherent advantages over the method of moments approach, in that its implementation requires much less computer memory and run time. As mentioned previously, to solve the integral equation inherently associated with the moment method approach requires large amounts of computer memory because it is necessary to store the entire interaction matrix in (3). Also, solving this large system of equations is very slow since the number of operations is proportional to the square of the number of elements in the matrix. Therefore, finite-difference methods allow more realistic models to be constructed, which can be analyzed over higher frequency ranges. One disadvantage of this method, however, is that its implementation necessitates modeling a certain region of the space surrounding the object, as well as the object itself. Thus, the computer program input demands of this technique may be greater than the moment method, where only the object need be considered.

Finite-difference methods usually treat the EM interaction with the body as a time domain problem in which the

source of EM energy is turned on at  $t = 0$ . Because the technique can be mathematically quite involved, only a brief overview is contained here; readers interested in a more detailed discourse are advised to consult the references [18]–[24]. While the specifics of the solution vary, generally speaking, after  $t = 0$ , the propagation, scattering, and absorption of the fields emitted by the EM source are simulated on a grid or mesh of cells by solving Maxwell's curl equations

$$\nabla \times E = -\mu_0 \frac{\partial H}{\partial t} \quad (4)$$

$$\nabla \times H = \epsilon \frac{\partial E}{\partial t} + \sigma E \quad (5)$$

in which finite-difference approximations are employed for both time and space derivatives. For example, if  $\Delta x$ ,  $\Delta y$ ,  $\Delta z$ , and  $\Delta t$  represent the space and time increments, respectively, and the positions of the vector components of the electric and magnetic field components are positioned according to the so-called Yee grid [18] as illustrated in Fig. 5, then the difference equation for one scalar equation associated with (4) can be written as

$$\begin{aligned} H_x(x, y + \Delta y/2, z + \Delta z/2; t + \Delta t/2) \\ = H_x(x, y + \Delta y/2, z + \Delta z/2; t - \Delta t/2) \\ + \frac{\Delta t}{\Delta z \mu_0} \\ \cdot [E_y(x, y + \Delta y/2, z + \Delta z; t) \\ - E_y(x, y + \Delta y/2, z; t)] \\ + \frac{\Delta t}{\Delta y \mu_0} [E_z(x, y, z + \Delta z/2; t) \\ - E_z(x, y + \Delta y, z + \Delta z/2; t)]. \quad (6) \end{aligned}$$

Naturally, five more similar equations can be determined for the other components ( $H_y$ ,  $H_z$ ,  $E_x$ ,  $E_y$ , and  $E_z$ ) of the EM field. As seen from (6), the evaluation of the electric and magnetic fields occurs at alternate half-time steps. Further, the new value of any component of the field at each grid point only depends on its previous value and the previous values of adjacent components of the other field. Thus, a solution is achieved by time-stepping through the entire grid.

The space in which the field must be computed is, in theory, unbounded. In reality, however, this is impossible because a computer can store and compute only a finite amount of data. To circumvent this problem, it is necessary to surround the object by a volume large enough to contain the object and impose some conditions which must be satisfied at the boundary walls. The idea is to create the numerical illusion of an infinite space. One approach is to impose the radiation boundary condition [21] on the exterior surfaces of the boundary. Because the field radiated (scattered) by the object must behave as a far-zone field for this condition to be valid, the boundary volume must be significantly larger than the object to avoid excessive re-

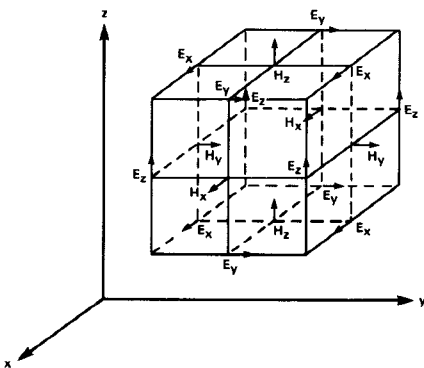


Fig. 5. Positions of the field components about a unit cell of the Yee lattice [18].

lections off the outer boundary. Another technique is to impose an absorbing boundary condition [24] on the walls.

Presently, the memory limitations of large main-frame computers restrict problem spaces (object plus surrounding volume) to typically around 25 000 or 30 000 cells, with an upper limit of 100 000 cells if more sophisticated programming is applied. Even with these upper limits, the spatial resolution available for modeling the interior detail of a biological body is restricted. This restraint can be circumvented by the application of a so-called expansion technique [23]. Basically, the expansion approach uses an initial computer run with a fairly coarse division of the problem space with the computed data being stored on disk. A certain portion of the body is then subdivided into a much finer division of cells and is called a subvolume. This becomes the problem space for a second computer run. Now only this subvolume is treated by imposing the same incident field conditions as the first run. In addition, interpolated tangential electric fields generated by the first run are imposed on the outer boundary of the subvolume. These tangential fields numerically mimic the response of the rest of the body, thereby ensuring that the subvolume response behaves as if the remaining portions of the body are still present. Obviously this process could be carried out several times. For example, the whole body of a human could be considered for the first run in which the head is coarsely modeled. The second run would replace the coarse head model with a much finer rendition of the head including detail such as the nose, eyes, brain, and skull. A third run might even be employed that focused on the intricate detail for the eyes.

While these finite-difference techniques yield transient solutions to Maxwell's equations, it is also possible to obtain continuous wave (CW) steady-state-type solutions. This can be accomplished by merely letting the time domain solution run for a period of time long enough to achieve steady-state conditions for a CW source turned on at  $t = 0$  [20]. On the other hand, since a pulsed waveform contains a spectrum of frequencies, it is possible to obtain spectral information about the body's SAR (such as presented in Fig. 3) over a large frequency range with only one execution of the computer program. This is achieved by the application of the Fourier transform in which the time

domain response is transformed to the frequency domain according to

$$F(\omega) = \frac{1}{2\pi} \int_{-\infty}^{\infty} f(t) e^{j\omega t} dt. \quad (7)$$

Because (7) cannot, in general, be analyzed analytically, it is necessary to numerically evaluate the integral by employing standard fast Fourier transform (FFT) routines. These procedures, however, are well documented, and most large computer systems have FFT subroutines available.

To determine the body's true CW response from transformed data requires careful consideration. From linear system theory, it is well known that the output of a system  $o(t)$  is related to the input  $i(t)$  by the system impulse response  $h(t)$  via

$$o(t) = \int_{-\infty}^{\infty} i(t - \tau) h(\tau) d\tau \quad (8)$$

with the Fourier transform given by

$$O(\omega) = I(\omega) H(\omega). \quad (9)$$

If  $I(\omega)$  represents the incident field and  $O(\omega)$  the observed response at a point in the body, then it is clear from (9) that  $H(\omega)$  is the desired CW response because it contains no spectral components of the source. In theory,  $H(\omega)$  could be determined by simply using a unit impulse for the incident field. However, this type of waveform poses severe problems when evaluating the FFT of (7) since  $H(\omega)$  does not, in general, go to zero as  $\omega$  approaches infinity. Consequently, the numerical solution would probably not converge. This problem can be alleviated by using an incident field that contains a finite spectral content, such as a damped sine waveform. Then  $I(\omega)$  will approach zero with increasing  $\omega$ , and the FFT technique will yield accurate information. Of course, (9) must be solved for  $H(\omega)$  after the FFT has been applied.

To determine the capabilities and limitations of the finite-difference technique as it applies to the human dosimetry problem, the U.S. Environmental Protection Agency (EPA) has supported the development of a computer code tailored for biological application and operation on the IBM 370/168 computer [25]. Fig. 6 illustrates a preliminary model comprised of cell sizes of  $4 \times 4 \times 6$  cm. The interior organs, bones, muscles, etc., were modeled to an accuracy as limited by the cell size, and the assigned permittivity values were appropriate for each tissue type. Note that the figure contains a volume which surrounds the object; the reasons for this volume were previously discussed. The entire problem space contains 15 000 cells and the body is comprised of approximately 1000 cells. It is important to realize that 1000 cells is not an upper limit for subdividing the body, and even with a relatively slow computer, such as the IBM 370/168, a body comprised of 10 000 cells is well within the computer's capacity. The 1000-cell model is primarily being used to ascertain the capabilities and limitations of the code. The cells within the broken line are of constant size. Those outside this boundary are allowed to increase in size by a factor of 1.25 for each step away from the dotted line. By assigning

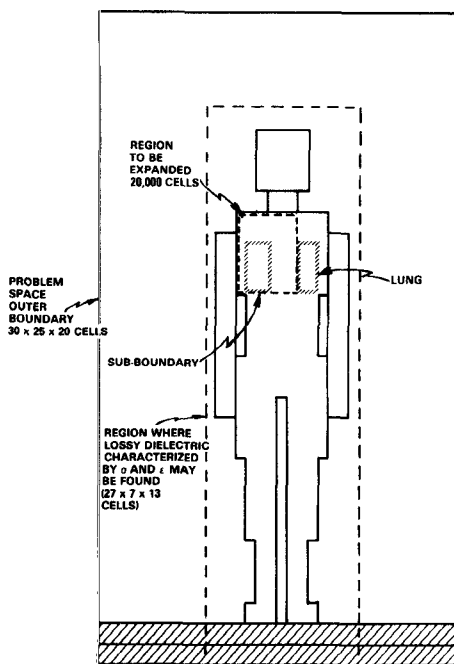


Fig. 6. Problem space for a human model [25].

appropriate permittivity values to the ground beneath the model's feet, it is possible to evaluate the effects of objects standing on the earth's surface. A perfectly conducting surface can also be utilized, as well as completely eliminating it for free-space calculations.

Fig. 7 illustrates views of the subboundary in which the lung and ribs are modeled in greater detail, using 20 000 cells with dimensions of  $1 \times 1 \times 1$  cm. The coarse model (Fig. 6) is used to compute the scattered tangential electric fields on the subboundary. The incident field utilized for the first calculation, as well as the tangential electric fields obtained from the first calculation, are then imposed on the subvolume for a second run. The finer grid of the second run, and consequently finer time steps, imply that the values for both the spatial and time points for the tangential fields on the subboundary must be determined by interpolation. Fig. 8 shows the time-domain SAR response at a central point in the lung when the incident electric field is a damped sine wave of the form

$$E_x^{\text{inc}} = E_o \sin 2\pi\omega t' e^{-\alpha t'} U(t') \quad (10)$$

where

$$\begin{aligned} t' &= \text{retarded time} = t - (z - z')/c, \\ z' &= \text{observation point}, \\ c &= \text{speed of light}, \\ U(t') &= \text{unit step function}, \\ \alpha &= 0.915 \times 10^9, \\ E_o &= 1 \text{ V/m}. \end{aligned}$$

It is seen that the incident field is propagating in the  $z$ -direction with its vector orientation in the  $x$ -direction. This corresponds to the electric-field vector being parallel to the major length of the body and propagating from the front to the back of the object. Note that this damped field

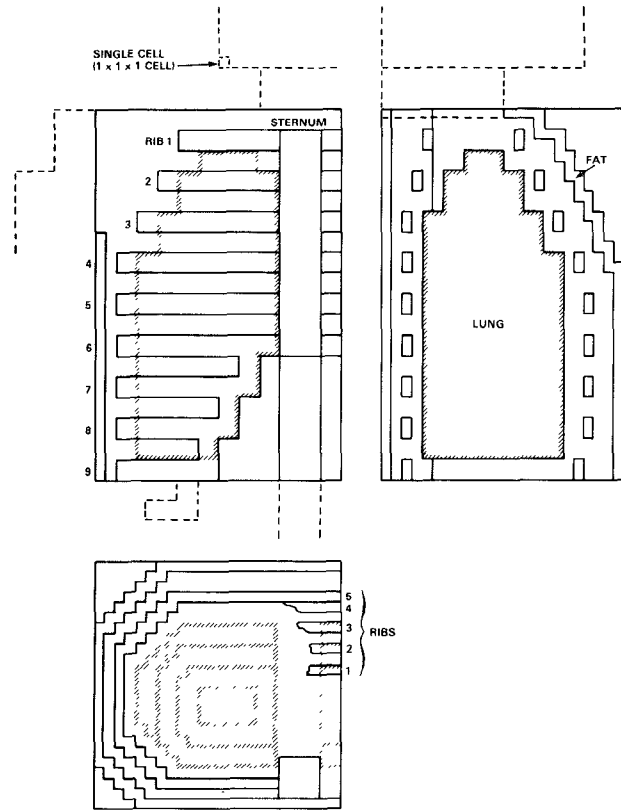


Fig. 7. Detailed model of lung region [25]. The top left figure contains a frontal view; the top right figure shows a section parallel to the sagittal plane taken through the center of the lung; and the bottom figure illustrates a transverse section taken through the center of the lung.

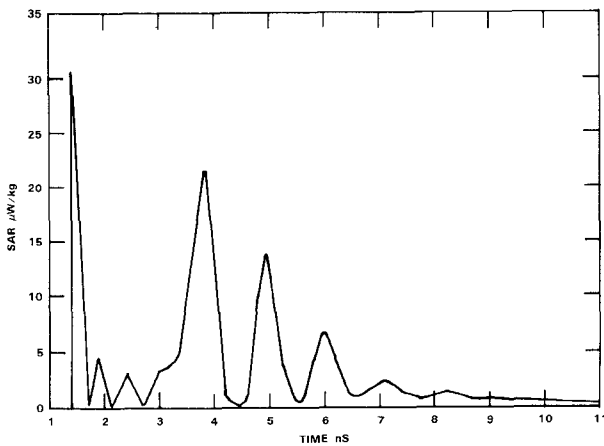


Fig. 8. Time-domain SAR response in the lung when the incident field is a damped sine wave oscillating at 915 MHz. The amplitude of the incident field is unity ( $E_o = 1$ ).

is turned on at  $t = 0$ , and is oscillating at 915 MHz. The SAR response contained in Fig. 8 was calculated by employing (1) after the electric-field response was determined via the finite-difference method. It is interesting to observe that the complexity of the shape of the response indicates that a significant amount of internal reflections of the wave occur inside the body. Because tissue is a lossy material, the internal field oscillates only for a few cycles and then is

rapidly damped out. The approximate 1-ns lag time before the field begins to build up inside the body is due to the incident wave being launched at  $t = 0$  at the outer boundary of the problem space. Therefore, a finite amount of time is needed before the wave impinges on the body. This time-domain response can be transformed via an FFT routine to yield frequency-domain information over a wide frequency range.

It is important to emphasize that the curve contained in Fig. 8 represents preliminary data whose accuracy is not yet established. These results are presented primarily to illustrate the finite-difference approach. The method must yet be compared with experimental results to ascertain the magnitude of error associated with the computed SAR values.

### III. THERMOREGULATORY MODELS

Since the human body possesses a complex thermoregulatory system to maintain a relatively constant temperature of the body core, any heat transfer model of the body must not only consider the standard modes of heat transfer (conduction, convection, and radiation), but also the thermoregulatory feedback mechanisms of vasoconstriction, shivering, vasodilation, and sweating. The mechanisms of vasoconstriction and shivering are called upon when the body's core temperature drops below a given set point, while vasodilation and sweating provide regulation when the body's core temperature rises above the set point. The combination of these mechanisms, along with stored thermal energy in the form of tissue capacitance, produces a relatively isothermal environment for the body's inner core.

Several investigators have developed mathematical models to calculate the thermal response of the human body when subjected to different environmental conditions or levels of exercise. The same basic approach can be taken to develop a model to simulate the effect of EM radiation. This model, however, must take into account that EM fields deposit energy nonuniformly in the human. The simple one-dimensional heat transfer models used in the past will not accurately simulate this condition. A short review of these previous attempts to model man will, nonetheless, provide good background for developing a more general model. No attempt will be made to provide an exhaustive literature survey of the existing models, since this has been undertaken elsewhere [26]–[28]. Rather, a brief historical overview will be given, along with a brief discussion of Stolwijk's model of thermoregulation. This model is highlighted since it appears to be widely accepted and has been modified by various researchers for specific purposes.

One of the earliest attempts at modeling the human body was made by Pennes [29], who developed a cylindrical model of a human limb. This model was first developed to simulate the human forearm, but was later generalized to any limb. The following factors were included in this model: 1) radial conduction, 2) metabolic heat generation, 3) convection to the blood, and 4) environmental exchange by convection, radiation, and evaporation.

A more rigorous analytical approach was taken by Hardy [30] to apply the laws of thermodynamics and heat transfer to the human system. This analysis included radiant exchange with the environment, thermal conduction through concentric cylinders, both natural and forced convection, and evaporation from the skin and lungs. The analysis was accompanied by experimental verification of a number of the calculated responses.

Machle and Hatch [31] introduced the concept of a core-and-shell model by comparing measured values of rectal and skin temperatures representing the core and shell temperatures used in the model. Empirical correlations for radiation, convection, and evaporation were experimentally developed for inclusion in this model. A modification by Kerslake and Waddell [32] extended the model to include the case of complete skin wetness due to sweating.

Wyndham and Atkins [33] further extended the core-and-shell model by introducing several concentric cylinders representing the different body layers. This model used a finite-difference technique to solve a set of resulting first-order differential equations by an analog computer. Smith and James [34] developed another analog model to study thermal stress in man. This model had the following characteristics: 1) metabolic heat production in the working muscles, 2) muscles insulated by a layer of subcutaneous tissue, 3) blood flow from the muscles to the skin, and 4) blood flow between different elements of the body and heart. This model considered radial conduction through three concentric cylinders and counter-current exchange between the arteries and veins, and it was verified experimentally.

Wissler [35], [36] modified the models of Pennes and Wyndham and Atkins and combined them to obtain a model of the entire human body. This model sub-divided the body into six elements: head, torso, two arms, and two legs. Each of these elements was assumed to have the following: 1) a uniformly distributed metabolic heat generation, 2) a uniformly distributed blood supply, 3) a composition of homogeneous materials, and 4) a geometry of isotropic cylinders. The effects of heat loss through the respiratory system and countercurrent heat exchange between the arteries and veins were also included. Recently, this model has been upgraded to better account for active physiological factors in thermoregulation, such as regional perfusion rates [37].

A major effort at modeling the entire human body was made by Stolwijk and associates at the John B. Pierce Foundation Laboratory. The initial effort by Stolwijk and Hardy [38] was composed of three cylindrical segments, one each for the head, trunk, and extremities. The trunk was divided into three concentric layers: skin, muscle, and core. The head and extremities were divided into only two concentric layers: skin and core. In this work, the concept of the body being composed of a controlled system and a controlling system was suggested. These investigators also did a rigorous review to determine accurate material properties of the human body. This model was then pro-

grammed for an analog computer and compared to experimentally developed parameters.

This model was then expanded by Stolwijk and Cunningham [39], Stolwijk [40], [41], and Stolwijk and Hardy [42] to include six segments: head, trunk, arms, hands, legs, and feet. All of these segments were composed of four layers: skin, fat, muscle, and core. The geometry of each was cylindrical, except the head, which was spherical. This model was programmed for a digital computer and included high metabolic heat production, sweating, blood flow to all layers, and convective and radiant exchange with the environment. Stolwijk's model has been adapted by several investigators to study special cases, such as Montgomery [43]–[45] to investigate the effects of man immersed in water.

Gordon *et al.* [46] extended and improved upon the basic ideas formulated by Stolwijk and Wissler to model the human temperature regulatory response after exposure in a cold environment. This model characterized the human body as 14 cylindrical and spherical segments with a cold exposure control system. The control of metabolism, skin blood flow, and muscle blood flow was achieved by utilizing feedback controller signals consisting of the head core temperature, mean skin temperature, and mean skin heat flux. The heat flux control signal was not included in previous models, but the results of this study indicate that it is important when modeling the human thermoregulatory response in cold environments.

Most recently, the basic models of Stolwijk and Wissler were combined to achieve high accuracy time-domain solutions by employing radial space intervals that are one hundredth of the radius of the various compartments of the body [47]. This simulation is very useful in calculating the response of human subjects to rapidly changing environments because the high degree of spatial resolution of the model allows large temperature gradients to be handled with a minimum of error.

#### *A. Modified Stolwijk Model*

Since the Stolwijk model tends to be the one most investigators have adapted for their own special needs, a succinct discussion of that model is included here. A more detailed mathematical description of the model is contained in [41], along with a listing of the program which is used to implement the model on a computer.

While Stolwijk's original model represented the body by six cylindrical segments, with heat flow from the core to the skin, the model considered here makes a minor modification to the original one by subdividing the body into fifteen segments [48]. Heat is also allowed to flow, not only from the core to the skin, but along the major axis of the body. This modification is useful when considering the effects of heat generation by EM deposition.

For thermal modeling purposes, Stolwijk considered the body to be composed of two systems: a controlling system and a controlled system. The controlled system can be modeled by a transient heat conduction model, with the

controlling system providing physiologically relevant thermal boundary conditions in order to maintain homeothermy.

1) *Controlled System*: Basically, the controlled system is a transient heat conduction model with internal heat generation and heat dissipation. The internal heat generation is caused by the body's metabolism (later, EM energy deposition will also be considered as an internal heat source). The internal heat dissipation is produced by convective exchange with the cardiovascular system and a combined convective and radiant exchange with the surrounding environment at the surface of the skin. The well-known heat transfer equation simulating this response is

$$\rho c (\partial T / \partial t) = \nabla (k \nabla T) + (1/V) (Q_M - Q_S - Q_R) \quad (11)$$

where

- $Q_M$  metabolic heat generation,
- $Q_S$  evaporative heat dissipation in the skin,
- $Q_R$  respiratory heat loss in the lungs,
- $\rho$  tissue density,
- $c$  tissue specific heat,
- $k$  tissue thermal conductivity,
- $T$  local tissue temperature,
- $t$  exposure time,
- $V$  tissue volume.

To solve for the heat transfer within the body, it is divided into several finite segments and (11) is applied to each segment. The model consists of 15 cylindrical segments and a sphere for the head, with each segment divided into 4 concentric layers: core, muscle, fat, and skin. As shown in Fig. 9, the neck, hands, and feet are approximated by single cylindrical segments, while the arms and legs are divided into 4 cylindrical segments and the trunk is divided into three segments. The radius and length of each of the cylindrical segments are based on dimensions for standard man [49]. Calculations of heat capacitance, thermal conductance, and density are based on the type of tissue, the surface area, and volume of each segment and layer. With this arrangement, the local temperature can be calculated at 100 positions throughout the body (the total number is actually 101 because the temperature of the central blood pool is also calculated).

In this model, the time and spatial derivatives are represented by finite-difference approximations, and the resulting system of equations is solved by an iterative procedure in which the initial temperatures are used to compute the temperatures a short time later. These new temperatures are then used to compute the temperatures at the new time and so on until thermal steady-state conditions are reached. The set of equations is first solved for a situation representing a resting man in a neutral environment of 30 °C ambient temperature and 30-percent relative humidity. For this calculation, the rate of blood flow is set at the

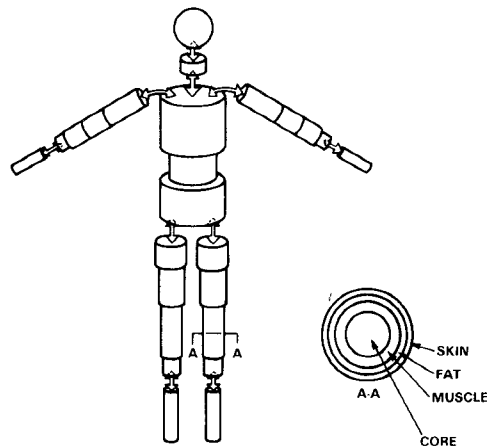


Fig. 9. The cylindrical model of man used for heat transfer calculations [48].

basal level and it is also assumed that no sweating occurred. The resulting steady-state temperature distribution is designated as the setpoint temperatures, and they are considered to be the temperatures which the thermoregulatory system attempts to maintain. These temperatures (listed in Table I) are also used as the initial temperatures for each of the nodes when (11) is solved for other conditions. Note that the table only contains 61 temperatures because the values for each leg and arm are equal. This may not be the case when EM absorption is considered.

Fig. 10 shows the relationship of the various thermal conductances associated with a typical segment which includes four nodes in the finite-element analysis. Each lumped conductance represents heat exchange with the other nodes. The quantities  $K_C$  and  $K_A$  represent the radial and axial conductances, respectively, whose values are determined by the layer and segment geometry and by tissue thermal conductivity [50]. Heat exchange between the skin and surrounding environment by convection and radiation is represented by the quantity  $H$ . The remaining elements, the  $BF$  terms, designate the amount of heat convectively exchanged by each node and the central blood pool. Because blood flow plays such an important role in heat transfer within the body, these terms will be discussed further. In Stolwijk's model, the blood flow rates to all segments, except the skin and muscle, are set to basal values. The muscle blood flow is controlled by the metabolic demand for oxygen. It is fixed at basal levels until increased oxygen needs of muscle activity, as a result from work or shivering, require the blood flow rate to be increased. The skin blood flow is highly dependent upon the thermal state of the body. Active vasodilation, along with increased sweating, represents the body's major adjustments to heat loads. An empirical relation for local skin blood flow is given by the expression

$$BF_i = \frac{[BFB_i + K_i \cdot DILAT]2^{(T_i - T_{i, \text{set}})/6}}{1 + \beta_i \cdot STRIC} \quad (12)$$

TABLE I  
SET-POINT TEMPERATURES (°C) [55]

Segment	Core	Muscle	Fat	Skin
Head	36.95	35.49	35.24	35.01
Neck	37.09	36.29	35.31	34.48
Upper trunk	36.86	36.53	35.02	34.14
Middle trunk	36.92	36.24	34.86	34.17
Lower trunk	36.92	36.46	34.99	34.16
Upper humerus	35.50	34.32	33.63	33.39
Lower humerus	35.51	34.32	33.63	33.39
Upper forearm	35.36	34.23	33.58	33.36
Lower forearm	34.83	33.99	33.45	33.43
Hand	35.84	35.66	35.58	35.46
Upper thigh	36.91	35.62	34.63	34.32
Lower thigh	36.53	35.31	34.54	34.30
Upper calf	36.39	35.22	34.50	34.29
Lower calf	35.65	34.80	34.34	34.21
Foot	35.61	35.39	35.30	35.17
Central blood	36.72	--	--	--

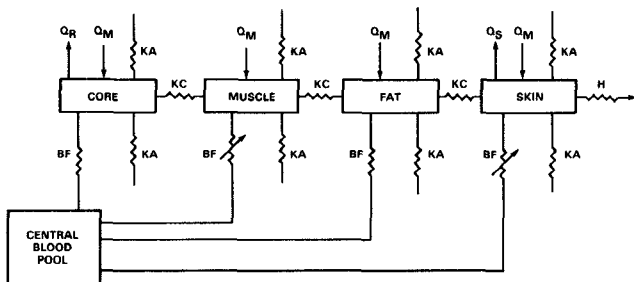


Fig. 10. Block diagram for one segment of the thermal model [48].

where

$BFB_i$  local basal blood flow rate,  
 $T_i$  local skin temperature,  
 $T_{i, set}$  local skin set-point temperature (see Table I),  
 DILAT total controller command for skin vasodilation,  
 STRIC total controller command for skin vasoconstriction,  
 $K_i$  fraction of DILAT command applicable to the skin of segment  $i$ ,  
 $\beta_i$  fraction of STRIC command applicable to the skin of segment  $i$ .

In the equation, the terms DILAT and STRIC are controller equations which will be discussed later. The weighted vasodilation command  $K_i \cdot \text{DILAT}$  is added to the basal blood flow in order to increase skin blood flow in response to increased body temperatures. The weighted vasoconstriction command  $\beta_i \cdot \text{STRIC}$  acts to reduce blood flow in response to decreased body temperatures. As will be shown later, the DILAT and STRIC commands are functions of both the integrated skin response and the difference between the instantaneous brain core temperature and its set-point temperature; however, it is also known that the local skin temperature affects the blood flow. Therefore, the exponential term in the expression accounts

for the local temperature effect. It doubles the blood flow rate for every 6 °C increase in local temperature above the set-point temperature and cuts the flow in half for a 6 °C drop in temperature. Note also that the controller commands DILAT and STRIC do not act simultaneously. If vasodilation occurs, then STRIC = 0; when vasoconstriction takes place, DILAT = 0.

The other heat exchange modes shown in Fig. 10 include: metabolic heat production  $Q_M$ ; heat loss by sweat evaporation on the skin  $Q_S$ ; and heat loss in the lungs  $Q_R$ . To calculate the respiratory heat loss, it is assumed that the expired air has come to thermal equilibrium with the upper trunk core temperature and is saturated with water vapor. This term enters (11) only at the node that represents the core of the upper trunk segment. The body has its own source of heat produced by metabolic activity. For the model, the metabolic rates of the core, fat, and skin segment are assumed not to vary from basal levels. In the muscle segments, the metabolic rate can be accelerated as a result of work activity and shivering. Shivering is initiated when the body is subjected to a sufficiently low ambient temperature (< 28 °C for a nude subject) and experiences a chill.

Heat lost due to sweating  $Q_S$  is a major avenue by which the body regulates internal temperatures. Several mathematical models have been proposed to calculate the heat loss by sweating. They are all empirical and attempt to give a best-fit to experimental data for various conditions. The equation utilized by Stolwijk takes the form

$$Q_{S,i} = (QB_{S,i} + S_i \cdot \text{SWEAT})2^{(T_i - T_{i, \text{set}})/10} \quad (13)$$

where

$QB_{S,i}$  basal evaporative heat loss,  
 SWEAT total controller command for sweating,  
 $S_i$  fraction of sweating command applicable to skin of segment  $i$ ,  
 $T_i$  local skin temperature,  
 $T_{i, \text{set}}$  local skin set-point temperature.

Note that the general form of this expression is very similar to (12). For a given value of the controller command SWEAT, it is evident that the skin sweats more at a higher local skin temperature than at a lower temperature. As will be explained later, SWEAT is a function of hypothalamus and mean skin temperatures; thus, the local sweating response is both an additive and multiplicative function of the local skin, core, and mean skin temperatures. The quantity  $S_i$  accounts for the fact that sweat production is not uniformly distributed over the skin's surface. A good background description of various sweating models can be found in [51].

2) *Controlling System:* It is well known that temperature-sensitive thermosensors exist both in the skin and in the hypothalamic area; however, the actual sensors have not been clearly identified morphologically. There have also been claims for sensors in other places in the body,

but these have not yet been clearly established. It is known that, when the body core (hypothalamus) is warmed, heat dissipating actions, such as sweating and dilation of the skin blood vessels, occurs. When the body core is cooled, it reacts with heat-generating responses, such as shivering and constriction of the peripheral blood vessels. On the other hand, a second set of sensors must exist because, if one enters either a hot or cold environment, sweating or shivering occurs before the core (hypothalamus) experiences any temperature rise or drop. In other words, the body takes corrective action long before an internal temperature increase or decrease occurs. This could only happen if there exist peripheral thermosensors on the skin to provide information about rapid changes in the external environment.

These thermosensors are either "warm" or "cold" receptors. Upon sudden warming, a "warm" receptor will produce electrical impulse signals that are carried to appropriate locations by neural pathways. A decrease in the production of signals occurs when the area is suddenly cooled. A "cold" receptor acts in the opposite fashion, in that it increases the production of signals when a drop in the local temperature occurs. The homeothermic control system is, therefore, comprised of thermosensors connected by afferent pathways to a hypothalamic controller in the brain, which, in turn, produces alterations in vasoconstriction, vasodilation, sweat production, and shivering via effector pathways.

Physical or engineering models of this controller system incorporate set-point or reference temperatures (see Table I), and a deviation between the set-point temperature and the actual temperature represents an error signal. The size of this error signal is directly related to the magnitude of the response. The relationship between the error signal and thermal response (vasoconstriction, vasodilation, and sweating) can be approximated by a general controller expression

$$\text{CONTROL} = \alpha_1(T_H - T_{H,\text{set}}) + \alpha_2 \sum \beta_i (T_i - T_{i,\text{set}}). \quad (14)$$

A controller expression for the shivering mechanism can be put into a somewhat similar form, but will not be given (see [41]). The term  $(T_H - T_{H,\text{set}})$  represents the difference between the instantaneous brain core temperature and its set-point temperature. It accounts for the thermoreceptors in the hypothalamus. The second quantity in the expression represents the total integrated difference between the skin temperature and the skin set-point temperature, where the summation is over all the skin nodes. The quantities  $\alpha_1$ ,  $\alpha_2$ , and  $\beta_i$  are empirical constants. Thus, the error signal is determined according to the values for  $(T_H - T_{H,\text{set}})$  and  $(T_i - T_{i,\text{set}})$ ; positive values are warm receptor outputs and negative values imply cold receptor outputs. This controller equation is used to affect the vasomotor response through the DILAT and STRIC commands in (12) and the sweating response via the SWEAT command in (13). If the error signal is positive, then the DILAT and SWEAT commands

are activated. A negative error signal implies that STRIC is activated; however, the value that is substituted into (12) is the magnitude of the error signal.

### B. Comparison with Experimental Data

Several studies, e.g. [41], [52], have been concerned with the experimental validation of the Stolwijk model for an exercising subject or a sedentary subject that is placed in a room at a controlled temperature and relative humidity, then transferred to a second room at different environmental conditions. These types of experiments allow the transient response of the model to be verified. Experimental data for transient conditions of the rectal and various skin temperatures, as well as cardiac output and evaporative heat loss, have been compared to the output for the model. In general, for warmer air temperatures ( $> 28^\circ\text{C}$ ), the predictions are fairly good. For example, Fig. 11 shows experimental data [53] for a human subject placed in an environmental chamber for 60 min at  $28.5^\circ\text{C}$  and 40-percent relative humidity. The subject was then transferred to a second chamber controlled at  $37.5^\circ\text{C}$  and 33-percent relative humidity, and then returned to the first chamber at  $28.5^\circ\text{C}$  and 41-percent relative humidity. It can be seen from these data that the rectal temperature  $T_R$  and metabolic heat production  $Q_M$  remain relatively constant, but the mean weighted skin temperature  $T_S$  and sweating rate  $Q_S$  were dramatically affected.

At colder temperatures, when shivering is activated, the agreement is not as good, especially when the subject has undergone exercise. The process of simulating thermoregulation during exercise in the cold may require refinement in the model. A remedy recommended by Stolwijk is to simply add additional layers in the muscle segments to reduce the errors involved when the temperature gradients are large [41]. However, the Gordon *et al.* model [46] indicates that a heat flux control signal, which is not contained in the Stolwijk model, may additionally be required to achieve satisfactory prediction accuracy for cold environments.

## IV. COMBINED MODELS

Because the Stolwijk thermoregulatory model has demonstrated good agreement between the computer prediction and experimental data, especially at warmer ambient air temperatures, it is possible to proceed with the utilization of this model for the thermal analysis of man in an EM field. The thermal loading due to energy absorbed from an EM field can be accounted for by merely adding another heat input term  $Q_{EM}$  to (11) such that

$$\rho c(\partial T / \partial T) = \nabla(k \nabla T) + (1/V)(Q_M + Q_{EM} - Q_S - Q_R) \quad (15)$$

and each node of Fig. 10 would now have  $Q_{EM}$ , as well as  $Q_M$  (metabolic heat production), for the heat input terms.

When a human is subjected to an EM field, the heat generation produced by the field is not uniformly deposited throughout the body. The one-dimensional heat

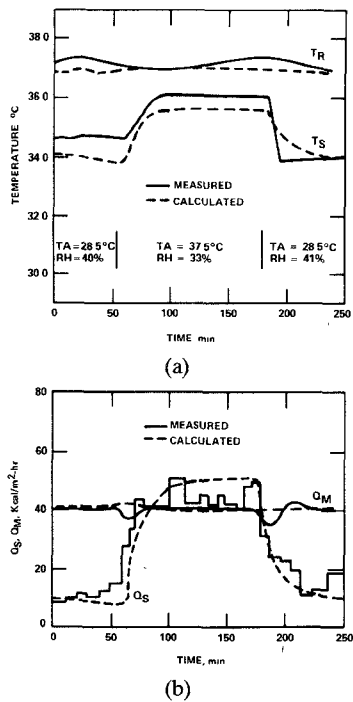


Fig. 11. A comparison of calculated [48] and measured [53] rectal ( $T_R$ ) and mean skin ( $T_s$ ) temperatures (a) and thermoregulatory response (b) versus time for a resting man subjected to changing environmental conditions.

transfer models, which only consider the flow of heat from the core to the skin, are not adequate. Thus, the controlling system for the feedback controls of vasoconstriction and vasodilation, sweating, and shivering probably can be adopted without major changes, but the controlled system must be modified to reflect the nonuniform deposition of EM energy by increasing the spatial resolution of the model. Generally speaking, this would require a three-dimensional solution to (15) in which heat flow for a cylindrical model could occur along and around a cylindrical segment, as well as from the core to the surface. This would, of course, require many more nodes than were utilized by the previously discussed 16-segment man.

#### A. Human Models

To date, there have been relatively few attempts to combine EM models and thermoregulatory models. In a study by Emery *et al.* [51], the thermal effects of a uniform deposition of EM energy were determined. Although this model may yield realistic values for averaged whole-body temperatures, the heating pattern produced by nonuniform deposition of energy will, in general, deviate substantially from that produced by uniform absorption. This deviation occurs because various parts of the body (head, arms, legs, etc.) selectively absorb different amounts of energy from the incident field because of the phenomenon of whole- and partial-body resonance (see Fig. 3). In another study, Guy *et al.* [54] used thermographic determinations of the distribution of EM energy in phantom models of man exposed to frequencies near whole-body resonance which were subsequently used to provide input for Emery's one-

dimensional thermal model [51]. While this model accounted for the nonuniformity in EM-energy deposition, it apparently did not account for heat flow along the major axis of the body. This is important, because the primary nonuniformity in the EM-energy deposition, especially for frequencies near whole-body resonance, will occur along the body's major axis. Thus, this model could be expected to overestimate the temperature profile in the body because the model allows heat flow to occur only from the core to the skin. In reality, as a result of localized EM-energy deposition, heat flow must also occur along the major length of the body.

The next attempt has been the work of Spiegel *et al.* [48], [55] and Spiegel [56] which has used block models to calculate the EM-energy deposition in the body with a two-dimensional extension of Stolwijk's model to determine the resulting thermal response. For the EM frequencies considered, the primary nonuniformity in the EM deposition occurred along the long dimension of the body, i.e., from the head to the feet. Therefore, this model allowed heat flow from the core to the skin as well as longitudinally along the major axis of the body. Heat flow around each segment was neglected, not only for the assumed circular symmetry of EM heat sources, but also because each segment in the thermal model has a constant thermal conductivity for a given radius. To calculate the EM absorption, a 70-kg standard man comprised of 180 cubical blocks (Fig. 1) of various sizes was utilized. The resulting EM energy deposition was input into the cylindrical heat transfer model (Fig. 9) in the following fashion. The 180 blocks of the EM block model were combined according to cross-sectional elements to form 32 composite layers. Once the EM energy deposition was determined for each composite layer, these layers were then combined to form a total layer with a thickness equal to the length of the cylindrical segment of the heat transfer model which represents the same position of the object. The energy deposited in the cylindrical segment is equal to the total energy contained in the combined layers.

To illustrate this model, Figs. 12 and 13 show selected temperature increases and thermoregulatory responses versus exposure time for a resting, nude man in a thermally neutral environment (temperature = 30 °C and relative humidity = 30 percent) during irradiation by a plane-wave at frequencies of 80 and 200 MHz. The electric-field vector is oriented parallel to the major axis of the body (i.e., *E*-polarization). Whole-body resonance occurs for the 80-MHz field, and partial-body resonance occurs in the arms at 200 MHz. The incident power density is 10 mW/cm<sup>2</sup>, which yields whole-body SAR's of 2.2 and 0.6 W/kg for the 80- and 200-MHz cases, respectively. Attention has been paid to the temperatures of the leg (80-MHz case) and arm (200-MHz case) because the EM model indicates high local SAR's in those regions. As can be seen, both the leg and arm temperatures exhibit greater increases than the rectal temperature. The increased thermoregulatory responses of sweating and vasodilation (increased skin blood flow) are able to keep the average body temperature

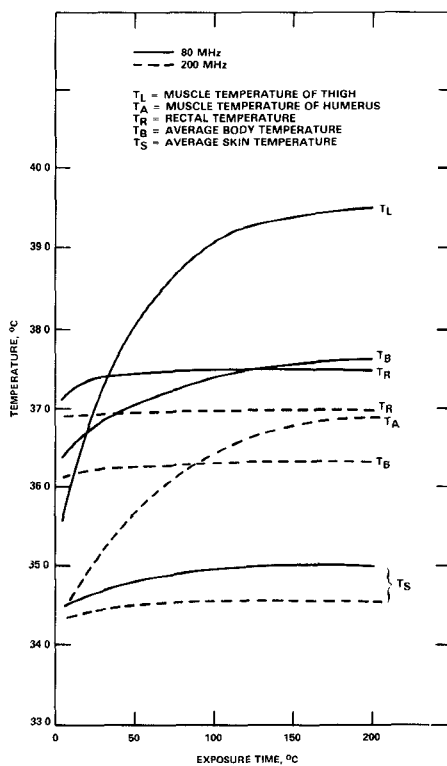


Fig. 12. Selected temperature responses as a function of time for plane-wave exposure conditions.  $T_{\text{air}} = 30^\circ\text{C}$ , relative humidity = 30 percent, air velocity = 0.1 m/s [55].

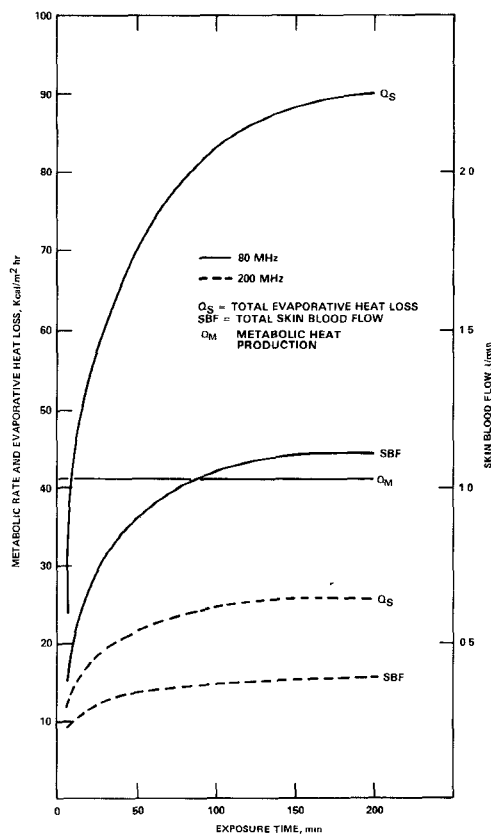


Fig. 13. Selected thermoregulatory responses as a function of time for plane-wave exposure conditions.  $T_{\text{air}} = 30^\circ\text{C}$ , relative humidity = 30 percent, air velocity = 0.1 m/s [55].

and average skin temperature from increasing significantly. Note that the evaporative heat loss and metabolic rate are plotted in units of  $\text{kcal}/\text{m}^2 \cdot \text{hr}$ . They can be converted into watts by multiplying by 2.15.

The major deficiency of this model is that the SAR distribution, as calculated by the EM model, exhibits considerable spatial variation over the body, and much of this variation was averaged out when it was transferred to the thermal model. Thus, the thermal model needs to be improved by increasing the number of cells or compartments to match the spatial resolution of the EM model. Another problem is that the model did not include the effects of increased local blood perfusion rates for tissues that are heated to temperatures in excess of  $40^\circ\text{C}$ . It is believed that internal tissues respond to local temperatures in excess of around  $40^\circ\text{C}$  by increasing blood flow; altered tissue blood flow rates do not, in general, exist in a detailed fashion because, with conventional heat loads, temperatures in excess of  $40^\circ\text{C}$  rarely occur in healthy humans.

Another interesting application [57] of Stolwijk's model was concerned with the model's prediction when a significant amount of EM energy was deposited in the hypothalamic region. In this study, a 1-cm-radius sphere was used to approximate the hypothalamus, and it was included in the model by adding another compartment in the head. The simulated EM energy deposition was accounted for by adding it to the metabolic heat input term for the hypothalamus. Fig. 14 shows the temperature difference between the simulated hypothalamic region and the surrounding brain tissue versus incident power density, in which the EM absorption term  $Q_{EM}$  of (15) is equal to 0.04 W for every 10 mW/cm<sup>2</sup> of incident power density. The results of this figure serve to point out that a hot spot can indeed occur in the head. The thermoregulatory system cannot eliminate the temperature gradient between the tissues; it can only lower both temperatures simultaneously. These temperature increases are kept reasonably low because of the fairly high blood-flow rates in the brain. It is important to reiterate that the hypothalamus is the thermoregulatory control center, and the heat dissipating mechanisms of sweating and vasodilation are strongly activated by even a small increase in hypothalamic temperature. The mathematical simulation of this response is through the controller commands of SWEAT and DILAT [see (14)]. As a consequence of increased sweating and vasodilation, a somewhat unexpected result occurs when EM energy is deposited solely into the hypothalamus: the body temperatures decrease from their initial values. Evidently, this happens because the total body heat loss by sweating exceeds the total heat input from the EM field. This phenomenon is illustrated in Fig. 15 for the trunk core.

Finally, two new models have been presented recently. In one study [58], an inhomogeneous thermal block model of man composed of 476 cubical cells was described. Partitioning of the various tissue types throughout the model was done according to anatomical cross-sectional data. This model's major improvement over previous mod-

els is that it can provide a more detailed temperature distribution inside the body because of the greater spatial resolution it affords. Another improvement is the inclusion of altered tissue blood flows for tissues that are heated in excess of 40 °C. The other study [59] used the Wissler thermal model [36] in conjunction with a 180-cell EM model [9]. To date, this model incorporates the most advanced treatment of convective heat transfer by blood.

### B. Animal Models

As stated above, the heat transfer and thermoregulatory models yield numerical data which compare reasonably well with experimental data based on specific environmental conditions. However, even though the inclusion of EM induced-heat sources in the thermal models is straightforward, the deposition of these heat sources is very unique vis-a-vis the heat load produced by external temperature or exercise. As a consequence, certain deficiencies may exist in the thermoregulatory model which are not important for more conventional heat loads. For example, it has been previously stated that internal tissues may respond to local temperatures in excess of around 40 °C by increasing blood flow above basal levels. The accurate simulation of this phenomenon is important because Fig. 12 illustrated that local SAR's during whole-body EM exposure can drive localized temperatures near 39–40 °C without a significant increase in the average body temperature. This localized hyperthermia effect is not as important when considering conventional heat loads because temperatures in excess of 40 °C have been rarely measured in healthy humans.

Empirical relations for these altered tissue blood flows have been utilized [58], but lack of experimental verification of the flow rates limits the predictive value of the combined EM-thermal models. Even if this localized hyperthermia problem is set aside, the critical question of the accuracy of the simulation models for small localized temperature increases cannot be definitively answered at this time because no experimentation has taken place. It is not likely that quantitative experimentation with human subjects will occur because of ethical considerations and difficulties associated with human exposure to EM radiation. Therefore, an alternate approach is to model an animal and then perform the necessary thermophysiological experiments on actual animals.

To that end, one study has been initiated in which the squirrel monkey has been chosen as a surrogate to study the accuracy of the combined models [60]. The squirrel monkey is a sweating, nonpanting primate whose major route of heat loss is through the skin. Their thermoregulatory system is similar to man's, albeit they do not sweat over their entire body surface, but sweat primarily on the palms of the hands and the soles of the feet. In addition, their tail is a very effective heat dissipator, a mechanism not available to man. The verification of a squirrel monkey model based on experimental data acquired from monkeys would provide a strong case for verification of the human model.

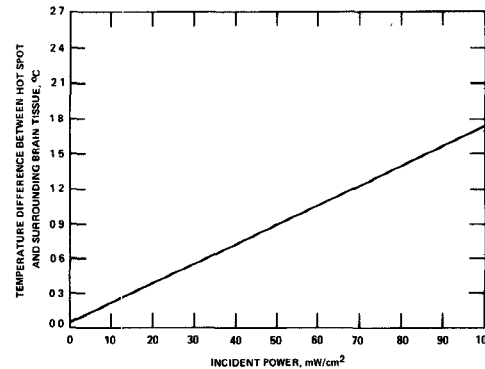


Fig. 14. Temperature difference between hot spot and surrounding brain tissue versus power density.  $T_{\text{air}} = 29$  °C, relative humidity = 10 percent, air velocity = 0.1 m/s [57].

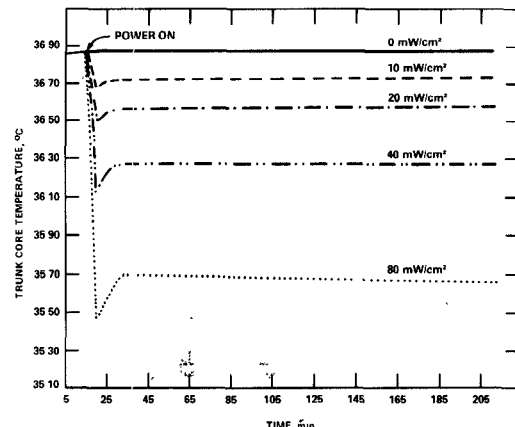


Fig. 15. Trunk core temperature versus time for exposure at different power densities. Power is turned on at the 15th minute.  $T_{\text{air}} = 29$  °C, relative humidity = 10 percent, air velocity = 0.1 m/s [57].

Fig. 16 shows a side view of the preliminary block model representation of the squirrel monkey. The model has core, muscle, skin, and fur layers, and is comprised of around 1000 rectangular blocks. The shaded region represents the core and the unshaded blocks represent muscle; the skin and fur layers were not drawn because they are very thin relative to the other layers. The model represents a squirrel monkey in a sitting position because, ultimately, the calculations will be compared to experimental data for an animal in this position.

The percentage of core, muscle, and skin was scaled volumetrically from human anatomical information. Blood-flow rates were scaled from human data by comparing cardiac output, except for the tail blood flow, which was scaled from published rat tail blood-flow data. Metabolic rates were obtained from published literature and distributed proportionately as in the human model, except for the tail. For lack of better information, the metabolic rate for the tail was assumed to be similar to that of the arm. The vasomotor (skin vasodilation and vasoconstriction) and sweating responses were scaled from Stolwijk's human model.

The implementation of this thermal model on a computer required around 5000 conductors to account for the various modes of heat transfer (see Fig. 10). Fig. 17 shows

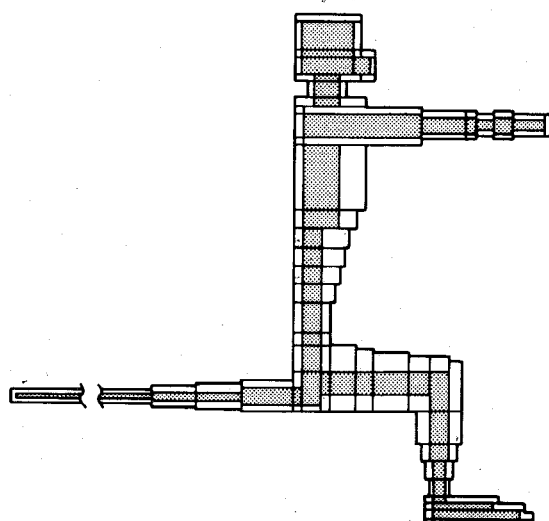


Fig. 16. A side view of the block model of a squirrel monkey in cross section taken through the sagittal plane of the body and the midlines of the arms and legs [60].

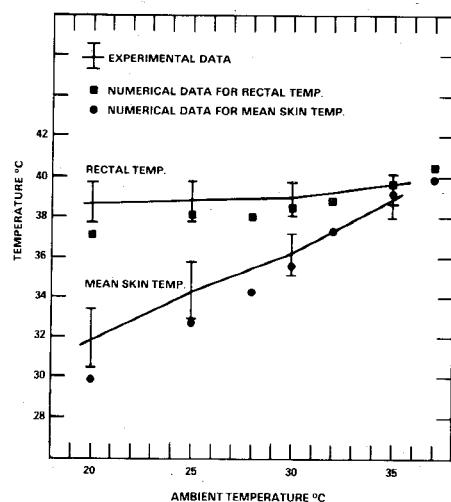


Fig. 17. A comparison of calculated [60] and measured [61] rectal and mean skin temperatures in a squirrel monkey versus ambient temperature. Relative humidity = 50 percent and air velocity = 0.1 m/s for the calculations.

the comparison of the calculated steady-state rectal and mean skin temperatures with experimental data [61] for different ambient temperatures and no EM heat input. The numerical values approximate the experimental data reasonably well. The major discrepancy occurs for lower ambient temperatures, but the reasons for this are not clear at this time. Further work is being directed at comparing the numerical results with experimental data when the model is irradiated by an EM field.

## V. CONCLUSION

Various EM dosimetric, thermoregulatory, and combined models were discussed. The latest EM models, although relatively crude in comparison to the human body, can, nonetheless, provide useful information about local

SAR's. Newer models, which will be most likely based on finite-difference methods, can be expected to increase resolution significantly over the next few years. These procedures, coupled with expansion techniques, will probably allow fairly intricate details of the body to be modeled with spatial resolution on the order of 1 cm<sup>3</sup>.

Likewise, the current heat transfer and thermoregulatory models are rudimentary approximations to a complex biological system, and they probably can, at best, predict gross effects and trends when EM deposition is included as a heat input term in the models. It can be expected that the finite-element solutions to the heat transfer equation will achieve spatial resolution comparable to what is achieved with the EM models. However, it may be difficult to determine appropriate parameter values for some of the empirical relations for the mathematically simulated thermoregulatory control system. For example, knowledge of blood flow to different portions of the body is now known with the necessary precision when the body is subdivided into several thousand cells.

In summary, the current mathematical models for predicting EM deposition and the resulting thermal response of the human body are not yet complete. It may be expected, however, that the human models will continually evolve into ever more sophisticated models with greater predictive capability and accuracy. In order to validate the models, animal models should be developed concurrently and tested for accuracy with relevant thermophysiological data. As physical and biological researchers combine their talents to meet these challenges, the growth of the knowledge in this area will be tremendous.

## ACKNOWLEDGMENT

The editorial contributions of Drs. J. A. Elder and J. W. Allis of the U.S. Environmental Protection Agency are gratefully acknowledged.

## REFERENCES

- [1] C. H. Durney, "Electromagnetic dosimetry for models of humans and animals: A review of theoretical numerical techniques," *Proc. IEEE*, vol. 68, no. 1, pp. 33-40, 1980.
- [2] O. P. Gandhi, "State of the knowledge for electromagnetic absorbed dose in man and animals," *Proc. IEEE*, vol. 68, no. 1, pp. 24-32, Jan. 1980.
- [3] —, "Electromagnetic absorption in an inhomogeneous model of man for realistic exposure conditions," *Bioelectromagn.*, vol. 3, no. 1, pp. 81-90, 1982.
- [4] C. M. Weil and J. B. Kinn, "Advances in experimental exposure methods and dosimetric techniques used in radio-frequency radiation biological effects studies," *Proc. IEEE*, vol. 17, no. 2, pp. 222-231, 1983.
- [5] A. W. Guy, M. D. Webb, and C. C. Sorenson, "Determination of power absorption in man exposed to high frequency electromagnetic fields by thermographic measurements on scale models," *IEEE Trans. Biomed. Eng.*, vol. BME-23, no. 3, pp. 361-371, 1976.
- [6] R. G. Olsen, "Far-field dosimetric measurements in a full-sized man model at 2.0 GHz," *Bioelectromagn.*, vol. 3, no. 4, pp. 433-441, 1982.
- [7] D. E. Livesay and K. Chen, "Electromagnetic fields induced inside arbitrary shaped biological bodies," *IEEE Trans. Microwave Theory Tech.*, vol. MTT-22, pp. 1273-1280, 1974.
- [8] K. M. Chen and B. S. Guru, "Internal EM field and absorbed power density in human torsos induced by 1-500-MHz EM waves," *IEEE Trans. Microwave Theory Tech.*, vol. MTT-25, pp. 746-755, 1977.

[9] M. J. Hagmann, O. P. Gandhi, and C. H. Durney, "Numerical calculation of electromagnetic energy deposition for a realistic model of man," *IEEE Trans. Microwave Theory Tech.*, vol. MTT-27, no. 9, pp. 804-809, 1979.

[10] O. P. Gandhi, M. J. Hagmann, and J. A. D'Andrea, "Part-body and multi-body effects on absorption of radio-frequency electromagnetic energy by animals and by models of man," *Radio Sci.*, vol. 14, no. 65, pp. 15-21, 1979.

[11] R. F. Harrington, *Field Computation by Moment Methods*. New York: Macmillan, 1968.

[12] M. J. Hagmann, O. P. Gandhi, J. A. D'Andrea, and I. Chatterjee, "Head resonance: Numerical solutions and experimental results," *IEEE Trans. Microwave Theory Tech.*, vol. MTT-27, no. 9, pp. 809-813, 1979.

[13] I. Chatterjee, M. J. Hagmann, and O. P. Gandhi, "Electromagnetic energy deposition in an inhomogeneous block model of man for near-field irradiation conditions," *IEEE Trans. Microwave Theory Tech.*, vol. MTT-28, pp. 1452-1459, 1979.

[14] K. Karimullah, K. M. Chen, and D. P. Nyquist, "Electromagnetic coupling between a thin-wave antenna and a neighboring biological body: Theory and experiment," *IEEE Trans. Microwave Theory Tech.*, vol. MTT-28, pp. 1218-1225, 1980.

[15] H. Massoudi, C. H. Durney, and M. F. Iskander, "On the adequacy and accuracy of the block models of man in calculating SAR distributions," presented at the 3rd Annual Conf. of the Bioelectromagnetics Society, Wash. DC, Aug. 9-12, 1981.

[16] C. T. Tsai, H. Massoudi, C. H. Durney, and M. F. Iskander, "Improved calculations of SAR distributions in biological models," presented at the 5th Annual Conf. of the Bioelectromagnetics Society, Boulder, CO, June 12-17, 1983.

[17] D. H. Schaubert, D. R. Wilton, and A. W. Glisson, "A tetrahedral modeling method for electromagnetic scattering by arbitrarily shaped inhomogeneous dielectric bodies," *IEEE Trans. Antennas Propagat.*, vol. AP-32, no. 1, pp. 77-85, 1984.

[18] K. S. Yee, "Numerical solution of initial boundary value problems involving Maxwell's equations in isotropic media," *IEEE Trans. Antennas Propagat.*, vol. AP-14, no. 3, pp. 302-307, 1966.

[19] C. D. Taylor, D. H. Lam, and T. H. Shumpert, "Electromagnetic pulse scattering in time-varying inhomogeneous media," *IEEE Trans. Antennas Propagat.*, vol. AP-17, no. 5, pp. 585-589, 1969.

[20] A. Tafove and M. E. Brodwin, "Numerical solution of steady-state electromagnetic scattering problems using the time-dependent Maxwell's equations," *IEEE Trans. Microwave Theory Tech.*, vol. MTT-23, no. 8, pp. 623-630, 1975.

[21] K. S. Kunz and K. M. Lee, "A three-dimensional finite-difference solution of the external response of an aircraft to a complex transient EM environment: Part I-The method and its implementation," *IEEE Trans. Electromagn. Compat.*, vol. EMC-20, no. 2, pp. 328-333, 1978.

[22] R. Holland, L. Simpson, and K. S. Kunz, "Finite-difference analysis of EMP coupling to lossy dielectric structures," *IEEE Trans. Electromagn. Compat.*, vol. EMC-22, no. 3, pp. 203-209, 1980.

[23] K. S. Kunz and L. Simpson, "A technique for increasing the resolution of finite-difference solutions of Maxwell equations," *IEEE Trans. Electromagn. Compat.*, vol. EMC-23, no. 4, pp. 419-422, 1981.

[24] G. Mur, "Absorbing boundary conditions for the finite-difference approximation of the time-domain electromagnetic-field equations," *IEEE Trans. Electromagn. Compat.*, vol. EMC-23, no. 4, pp. 377-382, 1981.

[25] K. S. Kunz, "An EPA-based computer code implementation of lossy dielectric finite-difference techniques for predicting human microwave dosimetry with high spatial resolution," submitted as an EPA report, Research Triangle Park, NC, 1984.

[26] A. Shitzer, "Mathematical models of thermoregulation and heat transfer in mammals. A compendium of research," NASA TM-X-62172 (NTIS PC E03/MF A01), 75 pp., 1972.

[27] C. L. Hwang and S. A. Konz, "Engineering models of the human thermoregulatory system-A review," *IEEE Trans. Biomedical Eng.*, vol. BME-27, no. 4, pp. 309-325, 1977.

[28] J. A. J. Stolwijk, "Mathematical models of thermal regulation," *Ann. N. Y. Acad. Sci.*, vol. 33, pp. 98-106, 1980.

[29] H. H. Pennes, "Analysis of tissue and arterial blood temperatures in the resting human forearm," *J. Appl. Physiol.*, vol. 1, pp. 93-122, 1948.

[30] J. D. Hardy, "Heat transfer," in *Physiology of Heat Regulation*, L. H. Newburgh, Ed. Philadelphia: W. B. Saunders, 1949, pp. 78-108.

[31] W. Machle and T. F. Hatch, "Heat: Man's exchanges and physiological responses," *Physiol. Rev.*, vol. 27, pp. 200-227, 1947.

[32] D. M. Kerslake and Waddell, "The heat exchange of wet skin," *J. Physiol.*, vol. 141, pp. 156-163, 1958.

[33] C. H. Wyndham and A. R. Atkins, "An approach to the solution of the human biothermal problem with the aid of an analog computer," in *Proc. 3rd Int. Conf. Medical Electronics*, London, England, 1960.

[34] P. E. Smith and E. W. James, "Human responses to heat stress," *Arch. Environ. Health*, vol. 9, pp. 332-342, 1964.

[35] E. H. Wissler, "Steady-state temperature distribution in man," *J. Appl. Physiol.*, vol. 16, pp. 734-740, 1961.

[36] —, "A mathematical model of the human thermal system," *Bull. Math. Biophys.*, vol. 26, pp. 147-166, 1964.

[37] —, "Mathematical simulation of human thermoregulatory behavior," *Am. Soc. Mech. Eng.*, Houston, TX, 1981.

[38] J. A. J. Stolwijk and J. D. Hardy, "Temperature regulation in man—A theoretical study," *Pflugers Arch.*, vol. 291, pp. 129-162, 1966.

[39] J. A. J. Stolwijk and D. J. Cunningham, "Expansion of a mathematical model of thermoregulation to include high metabolic rates," NASA CR-92443 (NTIS N69-16568) Washington, DC, 133 pp., 1968.

[40] J. A. J. Stolwijk, "Expansion of a mathematical model of thermoregulation to include high metabolic rates," NASA CR-102192 (NTIS NTD-19831), Washington, DC, 120 pp., 1969.

[41] —, "A mathematical model of physiological temperature regulation in man," NASA CR-1855 (NTIS N71-33401), Washington, DC, 76 pp., 1971.

[42] J. A. J. Stolwijk and J. D. Hardy, "Control of body temperature," in *Handbook of Physiology—Reactions to Environmental Agents*, D. H. K. Lee, Ed. Baltimore: Williams and Wilkins, ch. 4, 1977, pp. 45-68.

[43] L. D. Montgomery, "A simulation of heat transfer in man under immersed conditions," Ph.D. dissertation, UCLA, Los Angeles, CA, 1972.

[44] —, "A model of heat transfer in immersed man," *Ann. Biomed. Eng.*, vol. 2, pp. 19-46, 1974.

[45] —, "Analytic model for assessing the thermal performance of scuba divers," *J. Hydronautics*, vol. 8, pp. 108-115, 1974.

[46] R. G. Gordon, R. B. Roemer, and S. M. Horvath, "A mathematical model of the human temperature regulatory system—Transient cold response," *IEEE Trans. Biomedical Eng.*, vol. BME-23, no. 6, pp. 434-444, 1976.

[47] P. Smith and E. H. Twizell, "Extrapolation of Pade approximates in the closed-loop simulation of human thermoregulation," *Appl. Math. Modeling*, vol. 6, no. 2, pp. 81-91, 1982.

[48] R. J. Spiegel, D. M. Deffenbaugh, and J. E. Mann, "Modeling heat transfer in man exposed to an electromagnetic field," Final Tech. Report No. 14-9239, Southwest Research Institute, San Antonio, TX, 106 pp., 1979.

[49] N. Diffrient, A. R. Tilley, and J. C. Bardagiy, *Humanscale 1/2/3*. Boston: MIT Press, 1974.

[50] H. S. Carslaw and J. C. Jaeger, *Conduction of Heat in Solids*. Oxford, Eng.: Clarendon Press, pp. 230-231, 1959.

[51] A. F. Emery, R. E. Short, A. W. Guy, and K. K. Kraning, "The numerical thermal simulation of the human body when undergoing exercise or nonionizing electromagnetic irradiation," *Trans. ASME, J. Heat Transfer*, vol. 98, pp. 284-291, 1976.

[52] S. A. Konz, C. L. Hwang, B. Dhiman, J. Duncan, and A. Masud, "An experimental validation of mathematical simulation of human thermoregulation," *Comput. Biol. Med.*, vol. 7, pp. 71-82, 1977.

[53] J. A. J. Stolwijk and J. D. Hardy, "Partitional calorimetric studies of responses of man to thermal transients," *J. Appl. Physiol.*, vol. 21, pp. 967-977, 1966.

[54] A. W. Guy, M. D. Webb, A. F. Emery, and C. K. Chou, "Determination of the average SAR and SAR patterns in man and simplified models of man and animals exposed to radiation fields from 50-2450 MHz and the thermal consequences," (Abstract), in *Symp. Biological Effects of Electromagnetic Waves*, XIX General Assembly, Int. Union of Radio Science, Helsinki, Finland., p. 13, 1978.

[55] R. J. Spiegel, D. M. Deffenbaugh, and J. E. Mann, "A thermal model of the human body exposed to an electromagnetic field," *Bioelectromagn.*, vol. 1, no. 3, pp. 253-270, 1980.

[56] R. J. Spiegel, "The thermal response of a human in the near-zone of a resonant thin-wire antenna," *IEEE Trans. Microwave Theory Tech.*, vol. MTT-30, no. 2, pp. 177-185, 1982.

[57] W. I. Way, H. Kritikos, and H. Schwan, "Thermoregulatory physio-

logic responses in the human body exposed to microwave radiation," *Bioelectromagn.*, vol. 2, no. 4, pp. 341-356, 1981.

[58] I. Chatterjee and O. P. Gandhi, "Thermal response of an inhomogeneous block model of man under near-field electromagnetic exposure conditions," presented at the 4th Annual Conf. of the Bioelectromagnetics Society, Los Angeles, CA, June 28-July 2, 1982.

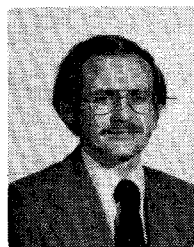
[59] E. H. Wissler, "Analytical study of human thermal response to whole-body microwave irradiation," presented at the 4th Annual Conf. of the Bioelectromagnetics Society, Los Angeles, CA, June 28-July 2, 1982.

[60] M. B. E. Fatmi and R. J. Spiegel, "Modeling the thermophysiological response of squirrel monkeys exposed to RF radiation," presented at the 5th Annual Conf. of the Bioelectromagnetics Society, Boulder, CO, June 12-17, 1983.

[61] J. T. Stitt and J. D. Hardy, "Thermoregulation in the squirrel monkey (*Saimiri sciureus*)," *J. Appl. Physiol.*, vol. 31, no. 1, pp. 48-54, 1971.

◆

Ronald J. Spiegel (M'73) was born in Cleveland, OH. He received the B.E.E. degree in 1964 from the Georgia Institute of Technology, Atlanta,



and the Ph.D. degree in electrical engineering in 1970 from the University of Arizona, Tucson.

From 1971 to 1972, he was a Post Doctoral Fellow in biomedical engineering at Duke University. In 1973, he joined the Boeing Aerospace Company, Seattle, WA, as a Research Engineer engaged in studies of nuclear electromagnetic pulse (EMP) effects on aeronautical electrical systems. From 1974 to 1976, he was with IIT Research Institute, Chicago, IL, involved in research in bioelectromagnetics and extra low frequency (ELF) coupling, interference mitigation, and environmental studies associated with the Navy Seafarer antenna. From 1976 to 1980, he was with Southwest Research Institute, San Antonio, TX, performing research in a variety of areas, such as EMC, electrostatics, bioelectromagnetics, and electromagnetic geophysical exploration. He is presently with the U.S. Environmental Protection Agency, Research Triangle Park, NC, and is Chief of the Biological Engineering Branch. His current research efforts are concentrated in the area of microwave field interaction with biological media and dosimetric methods.

Dr. Spiegel is a member of the Eta Kappa Nu, Sigma Xi, the Bioelectromagnetics Society, and is a Registered Professional Engineer.

## Limitations of the Cubical Block Model of Man in Calculating SAR Distributions

HABIB MASSOUDI, MEMBER, IEEE, CARL H. DURNEY, SENIOR MEMBER, IEEE, AND MAGDY F. ISKANDER, MEMBER, IEEE

**Abstract**—Block models of man which consist of a limited number of cubical cells are commonly used to predict the internal electromagnetic (EM) fields and specific absorption rate (SAR) distributions inside the human body. Numerical results, for these models, are obtained based on moment-method solutions of the electric-field integral equation (EFIE) with a pulse function being used as the basis for expanding the unknown internal field.

In this paper, we first examine the adequacy of the moment-method procedure, with pulse basis functions, to determine SAR distributions in homogeneous models. Calculated results for the SAR distributions in some block models are presented, and the stability of the solutions is discussed. It is shown that, while the moment-method, using pulse basis functions, gives good values for whole-body average SAR, the convergence of the solutions for SAR distributions is questionable. A new technique for improving the spatial resolution of SAR distribution calculations using a different EFIE and Galerkin's method with linear basis functions and polyhedral mathematical cells is also described.

### I. INTRODUCTION

IN THE STUDY of the possible biological effects of electromagnetic (EM) radiation and in medical applications utilizing EM energy, it is important and desirable to determine the internal EM fields and specific absorption rate (SAR) distributions inside the human body. The existing models commonly used to predict the induced EM fields inside the human body are block models consisting of a limited number of cubical cells. Numerical results for these models are obtained based on moment-method solutions of the electric-field integral equation (EFIE) with a pulse function being used as the basis for expanding the unknown internal field [1]-[6]. Although the aforementioned models have provided significant information about the average whole-body and partial-body SAR's, there remains a need to obtain a detailed and more accurate SAR distribution in the human body. Specific suggestions have been made that such accurate numerical results may be obtained by using a larger number of mathematical cells and by further using inhomogeneous models to accurately represent the permittivity inhomogeneities in the body [6].

Manuscript received October 12, 1983; revised March 13, 1984. This research was supported by the USAF School of Aerospace Medicine, Brooks Air Force Base, TX 78235, under Contract F33615-79-C-0614.

The authors are with the Department of Electrical Engineering, University of Utah, Salt Lake City, UT 84112.